RSC Advances

ROYAL SOCIETY OF CHEMISTRY

www.rsc.org/advances

Optimized Li and Fe recovery from spent lithium-ion batteries via solution-precipitation method

Rujuan Zheng [a,b], Li Zhao[a], Wenhui Wang[a], Yuanlong Liu[a], Quanxing Ma[a], Deying Mu[a], Ruhong-Li[a] and Changsong Dai [*,a]

（[a] school of chemical engineering and technology，Harbin Institute of Technology, Harbin 150001，China. E-mail : changsd@hit.edu.cn）

（[b] College of Chemistry and Chemical Engineering，Qiqihar University, Qiqihar 161006，China）

A new process is optimized and presented for recovering and regenerating $LiFePO_4$ from spent lithium-ion batteries (LIBs). The recycling process reduces cost and secondary pollution caused by complicated separation and purification in spent LIBs recycling. $FePO_4 \cdot 2H_2O$ was recovered by dissolution-precipitation method from spent $LiFePO_4$ batteries. The effects of different surfactants (*i.e.* CTAB, SDS and PEG), which are added during solution, on the recovered $FePO_4 \cdot 2H_2O$ were investigated. Li_2CO_3 was precipitated by adding Na_2CO_3 into the filtrate. Then $LiFePO_4$/C material was synthesized by a carbon-thermal reduction method using recycled $FePO_4 \cdot 2H_2O$ and Li_2CO_3 as Fe, P, and Li sources. And the as-prepared $LiFePO_4$/C shows comparable electrochemical performance to that of commercial one.

Introduction

With the global economy's rapid development, the energy demand and consumption grow every day. There are many advantages of lithium-ion batteries (LIBs) because of their high working voltage, high energy density, small self discharge, long cycle life, convenient use and no memory effect reservoir.[1-3] LIBs have been widely used in consumer electronics and related electrical vehicles, and their production and consumption is increasing year by year.[4] And the rapid expansion of hybrid electric vehicles (EVs), plug-in hybrid electric vehicles (PHEVs) and pure EVs are now greatly increasing the consumption of LIBs. Large quantities of spent LIBs along with scraps will be generated due to their limited life spans and rapid updating of electronic products. The disposed LIBs in the environment are a waste of resources (e.g. Li salts), an environmental pollution, and has a negative factor of the energy crisis. Therefore, spent LIBs recovery is mandatory to preventing environmental pollution and resource

depletion.

As for battery recovery, many efforts have been focused on expensive and toxic metal contained cathode, for example $LiCoO_2$[5-10] and $LiNi_xCo_yMn_zO_2$[11-15]. However, little attention has been payed to the recovery of $LiFePO_4$, which has been widely employed as cathode of power LIBs. For example, in November 2015, $LiFePO_4$-based power LIBs shared 20.08% of Chinese market of pure electric passenger vehicles (i.e. 6230 cars have been selected to employed $LiFePO_4$-based power LIBs). More surprisingly, it share the 64.9% of the Chinese market of electric buses, that is, 14143 electric buses employed the $LiFePO_4$-based power LIBs.[16]

Under the circumstances, developing $LiFePO_4$ recovery technique is undoubtedly necessary, which is actually the focus of this work. This paper presents the whole diagram to recover the $LiFePO_4$ cathode, including the Li salt, iron salt and current collector. In addition, the high quality of recover materials were verified by using them as raw materials to synthesize high performance $LiFePO_4$/C (comparable to the commercial one). The optimized method presented in this work is environmental friendly, economically feasible, and scalable.

Experimental

Recovery of "cathode powder" from spent battery

Prior to recovery process, the spent LIBs were fully discharged and then disassembled. While the electrolyte was collected and recycled by supercritical method, the diaphragm was recycled by wind sieving, which take advantage of weight difference of electrodes and diaphragm. Then $LiFePO_4$ cathode sheet were crushed into about 2 cm^2 and heated at different temperatures ranging from 450-650 ^oC for 1 h, which not only removes the binders and the carbon in the electrod, but also oxidized Fe^{2+} into Fe^{3+} (which favors subsequent recovery of $FePO_4$). Powder can be separated from aluminum current collector via oscillation sieving.

Recovery of $FePO_4$

The mixed powder was dissolved by sulphuric acid in a reactor with continuously stirring at a speed of 500 rpm. The dissolution efficiency was optimized via removing insoluble impurities (e.g. residual graphite) and tuning the liquid - solid concentration acid ratio, reaction time, and temperature.

Ammonia was added to precursor solution in order to manipulate the pH value as 2. After filtration, the filter residue was washed with deionized water and then dried at 80 ^{o}C until reaching a constant weight, then the amorphous hydrated $FePO_4$ (samples A, without adding any surfactant in the precursor solution) was obtained.

The surfactant effect on the phase and morphology of precipitated $FePO_4 \cdot 2H_2O$ was investigated by adding 1wt % PEG-6000, CTAB and SDS in the precursor solution before adding ammonia, and the obtained amorphous hydrated $FePO_4$ are named as Sample B, C, and D, respectively.

To form $FePO_4$ with alpha quartz structure, the amorphous hydrated $FePO_4$ was then annealed at 700 ^{o}C for 5 h.

Recovery of Li_2CO_3

Li_2CO_3 was recovered by the following steps: concentrating the filtrate, bring to a boil, adding Na_2CO_3, filtering, and washing the filter cake thoroughly with deionized water.[17] Finally, the filter cake was dried at 80 ^{o}C until constant weight, and Li_2CO_3 was then obtained.

Re-synthesis of $LiFePO_4$ via carbon thermal reduction method using recycled $FePO_4$ and Li_2CO_3 as raw materials

To re-synthesize $LiFePO_4$, the recycled Li_2CO_3 (Li source) and $FePO_4$ (both Fe source and P source) with molar ratio of Li: Fe: P=1.05:1:1 were used as raw materials, and additional 20wt % sucrose (relative to weight of raw materials) was used carbon source to not only reduces the Fe^{3+} into Fe^{2+}, but also decomposes to a continuous carbon network for electrical conduction. These raw materials were first ball-milled together for 7 h with ethanol as a dispersant. The obtained mixture was heated to 300 ^{o}C under an argon atmosphere for 4 h. The mixture was then ground and heated to 700 ^{o}C under a reducing atmosphere for 10 h. The product (*i.e.* $LiFePO_4$/C) was ground

in an agate mortar for later use.

Characterization of materials

The concentration of P, Fe and Li is determined by inductively coupled plasma emission spectrometer (ICP-AES, American Perkin-Elmer Company Optima 5300 DV). The X-ray diffraction (XRD) patterns were collected using a D/max-gamma B X-ray diffractometer (Rigaku, Japan) with Cu Kα radiation (λ = 0.15405 nm), a voltage of 45 kV, a current of 50 mA. The patterns with 2θ ranging from 10 to 90 ^{o} were collected using a scan rate and step of 10 ^{o}/min and 0.02 ^{o}, respectively. The $FePO_4$ and $LiFePO_4$ products were characterized by infrared spectrometer (IR Magna 560 Nicolet companies in the United States). The morphology was examined by scanning electron microscope (QUANTA-200F American FEI Company) with working voltage of 10 kV. To study the effect of the annealing temperature on the $LiFePO_4$ cathode electrode, TG-DSC analysis (STA449F3, NETZSCH) was carried out with temperature ranging room temperature to 800 ^{o}C at a heating rate of 5 ^{o}C/min under air flow. XPS measurement was conducted on a PHI 5700 ESCA System (USA), using a monochromatised Mg-Ka radiation source. X-ray absorption near edge structure (XANES) spectroscopy of Fe K-edge was conducted by using the Soft X-Ray beamlines and Variable Line Spacing Plane Grating Monochromator (VLS-PGM) beamlines at the Canadian Light Source (CLS). XANES was recorded in the surface sensitive Total Electron Yield (TEY) or Fluorescence Yield (FY) using a Silicon Drift Detector (SDD) at SXRMB and a Micro-Channel Plate (MCP) detector at PGM.

Battery assembly and electrochemical test

The as-synthesized $LiFePO_4$/C was mixed with acetylene black and polyvinylidene fluoride (PVDF) at a mass ratio of 8:1:1 to form cathode slurry with N-methyl-2-pyrrolidone (NMP) as solvent. The slurry was coated on aluminum foil, vacuum dried at 100 ^{o}C for 10 h to get cathode sheet. The dry cathode sheet was then punched into 16 mm wafers, pressed at 1 MPa pressure for 3-5 min. The pressed wafers were vacuum dried at 120 ^{o}C for

10 h, and transferred to glove box for later use. The cathode sheet, lithium foil anode, and Celgard2300 microporous polypropylene diaphragm were assembled into CR2025-type coin cells in a glove box filled with high-purity argon. 1 mol/L $LiPF_6$ in a mixture of Ethylene carbonate (EC) and Dimethyl carbonate (DMC) (with volume ratio of 1:1) solution was used as electrolyte. The charge-discharge test was carried out through Neware Battery under different current densities (1 C=170 mA g^{-1}) in voltage ranges of 2.5-4.2 V.

Results and discussions

Effect of heat treatment on the spent $LiFePO_4$ electrode

In order to find an appropriate temperature for annealing, TG-DSC analyses of $LiFePO_4$ electrode was performed from room temperature to 800 °C under air flow at a heating rate of 5 °C/min. As shown in Fig. 1 a, the TG curve shows a weight loss of about 6.68 % the temperature increases from room temperature to 600 °C. The DSC curves show exothermic several peaks, which are around 421.8 °C, 475.5 °C, 579.2 °C, which can be due to the decomposition of binder and carbon in the electrode. According to the previous report[18] , the decomposition of the PVDF begins at 350 °C under an oxygen atmosphere and 600 °C is ideal for PVDF decomposition. The weight of the electrode has little change at temperature above 600 °C, indicating the completion of pyrolysis of binder and carbon. There is an obvious endothermic peak around 658.6 °C ascribed to the oxidation of aluminum foil, which is confirmed by the DSC/TG test of Al foil (shown in Fig. 1 b). Thus, we conclude that the optimum temperature of the heat treatment is 600 °C.

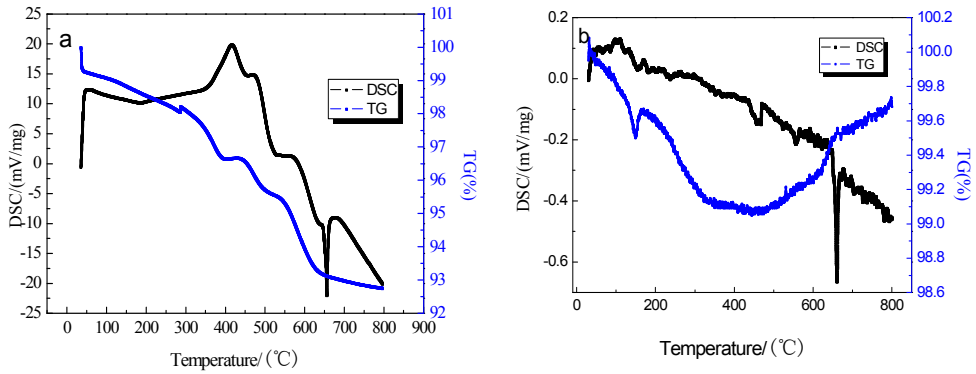

Fig. 1 TG-DSC curves of waste $LiFePO_4$ cathode sheet a and aluminum foil b

Table 1 shows the effect of annealing temperature on the color of electrode material and the degree of difficulty in separating materials from current collector via oscillating sieve separation. The separation effect of active material in the collection fluid demonstrates that the decomposition of the binder is not complete when the annealing temperature is lower than 550 °C. While when the temperature reaches up to 600 °C, the binder is completely decomposed and the active material can be easily separated from the current collector. The color change is due to the pyrolysis of the binder and the oxidation of Fe^{2+} to Fe^{3+} during annealing process in air. Fig. 2 shows XRD patterns of the electrode after the 1 h annealing process at different temperatures. Despite of the annealing temperature, the major phase of the material after heat treatment are monoclinic $Li_3Fe_2(PO_4)_3$ and Fe_2O_3, thus the oxidation of the LFP was expected to follow eqn 1. When the temperature reaches to 650 °C, diffraction peaks related to Al_2O_3 appears, indicating the oxidation of Al current collector (which is consistent with the analysis of TG-DSC curves) and exfoliation surface oxidized layer in the fluid flow. These result clearly demonstrate that the best annealing temperature should be 600 °C.

$$12LiFePO_4 + 3O_2 \rightarrow 4Li_3Fe(PO_4)_3 + 2Fe_2O_3 \quad \text{(eqn 1)}$$

Table 1 Effect of temperatures on the color and separation effect of the elecctrode

Temperature (°C)	450	500	550	600	650
Color	Dark brown	Light brown	Maroon	Brick red	Brick red
Amount of active materials separated from current collector	72%	84%	96%	100%	100%

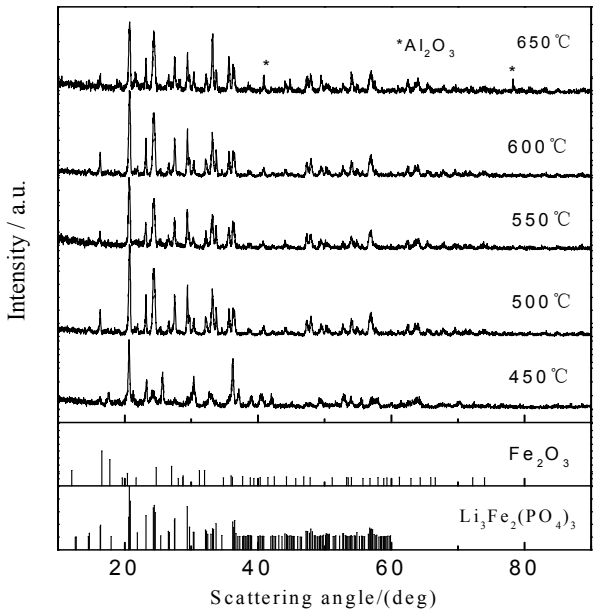

Fig. 2 XRD patterns of mixed powder after annealing at different temperature for 1 h

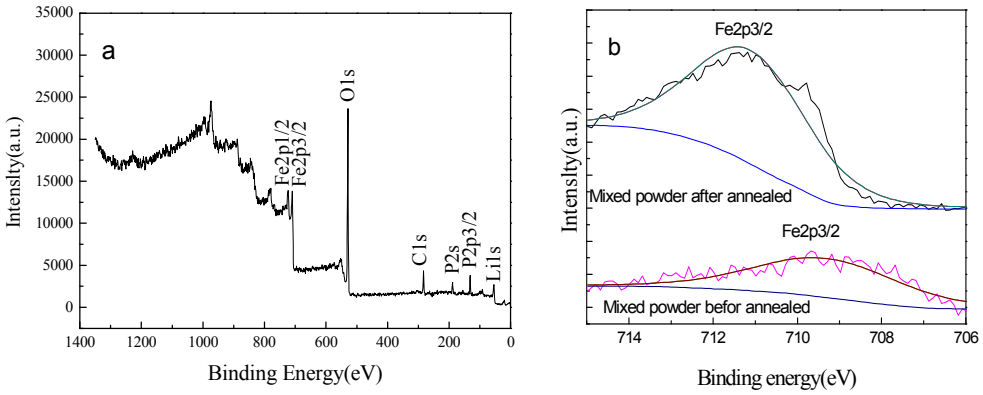

Fig. 3 XPS spectra of mixed powder before and after annealed at 600 ^{o}C for 1 h

The XPS spectrum (Fig. 3) of mixed powder both before and after annealing at 600 ^{o}C for 1 h show that the existence of O, C, Li, Fe, and P. The Li curve peaks at about 60eV. The fig.3 (b) XPS spectra Fe 2p3/2 spectra (Fig. 3 b) of mixed powder before and after annealing shows a binding energy of 709.7 and 711.3 eV, which corresponding to a valence number of +2 and +3, respectively.[19] therefore it can be assumed that Fe has completely oxidized into Fe^{3+}. ThereforeThus, it can conclude that the Fe^{2+} ion within $LiFePO_4$ can be completely oxidized into Fe^{3+} via annealing at 600 ^{o}C for 1h, which is consistent with analysis of XRD pattern before and after heat treatment.

Optimization of acid leaching process

In order to optimize conditions for acid leaching of mixed powder, the effects of sulfuric acid concentration, liquid to solid ratio, reaction time, and reaction temperature on the dissolution efficiency were investigated.

With a temperature of 60 ^{o}C, liquid to solid ratio of 10:1, reaction time of 4 h, the concentration of sulfuric acid was varies from 0.5 mol/L to 5 mol/L. As shown in Fig. 4 (a), with the increase of the concentration of sulfuric acid from 0.5 to 2.5 mol/L, the leaching efficiency of Li and Fe increased from 25 % to 97.2 % and from 46 % to 98.5 %, respectively; while further increasing the concentration of sulfuric acid above 2.5 mol/L shows negligible effect in leaching rate. Therefore, the best concentration of sulfuric acid leaching is 2.5 mol/L.

Fig. 4 (b) shows that the effect of the L/S ratio on the leaching rate when the concentration of sulfuric acid is 2.5 mol/L, the temperature is 60 ^{o}C, and the reaction time is 4 h. When the ratio of L/S reached 10, the leaching rates of Fe and Li 97.4 % and 96.1 %, respectively. Since the leaching rate shows little increases as further increasing of L/S, the optimal L/S (mL/g) ratio was determined to be 10.

Fig. 4(c) shows that the effect of the temperature on the leaching rate when the concentration of sulfuric acid is 2.5 mol/L, the L/S ratio of 10:1, and the reaction time is 4 h. When the temperature is lower than 60 ^{o}C, the leaching rate increases when reaction temperature increases; while when the temperature reaches above 60 ^{o}C the leaching rate shows little changes as the temperature increases. Therefore, the optimum leaching temperature is 60 ^{o}C .

Fig 4(d) shows that the effect of the reaction time on the leaching rate when the concentration of sulfuric acid is 2.5 mol/L, the temperature is 60 ^{o}C, and the L/S ratio of 10:1. Similar to previous discussion, the optimal extraction time was determined to be 4 h.

It can be concluded that the optimal leaching efficiency (*i.e.* 97 % and 98 % for Li and Fe, respectively) can be achieved when the sulfuric acid concentration, L/S, temperature and time is 2.5 mol/L, 10mL/g, 60 ^{o}C and 4 h,

respectively.

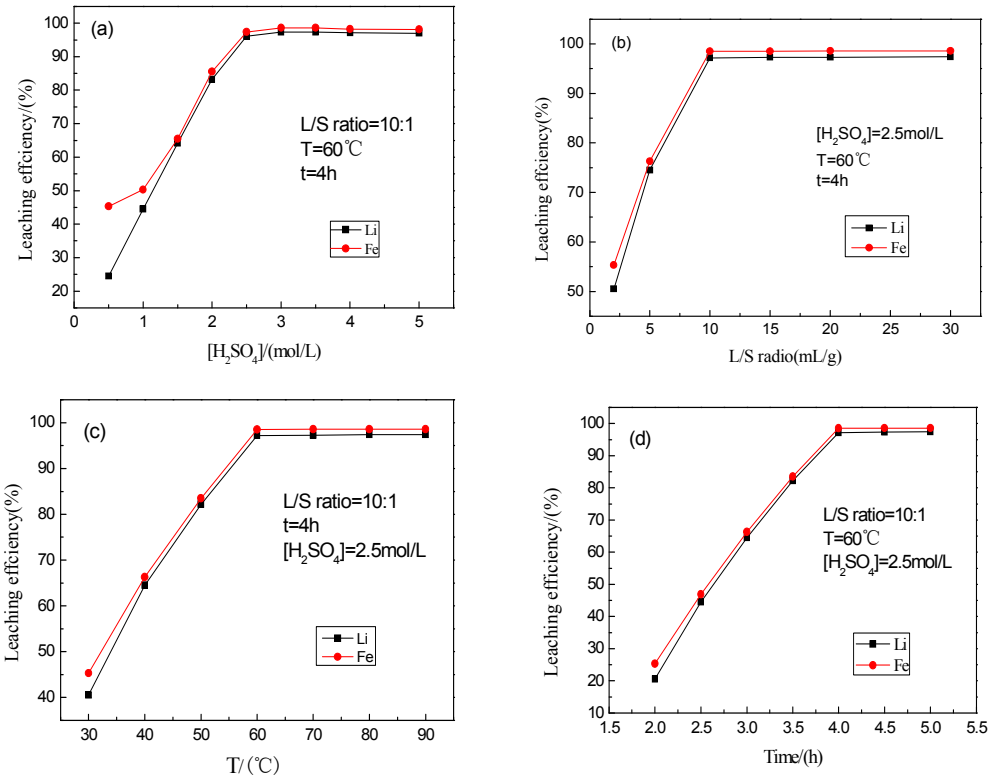

Fig. 4 Effect of sulfuric acid concentration, L/S ratio, temperature and time on the leaching of Fe and Li from battery powder

Compositional and structural analysis of the "$FePO_4$"

pH value is known as the key factor that controls the precipitation of $FePO_4$, thus will be investigated in the following part. When the pH > 1, the solution begins to precipitate. As shown in Fig. 5, the Fe/P molar ratio (analyzed by ICP-AES) in the precipitation increases gradually accompanied with the increase of the pH value. When the pH value was adjusted to between 1.9 and 2.1, Fe/P molar ratio analyzed to be 0.961-1.008, which is consistent with the molar ratio in $FePO_4$. Therefore, the best pH value for "$FePO_4$" precipitation is tentatively set to be 2 ± 0.5 in the control experiment.

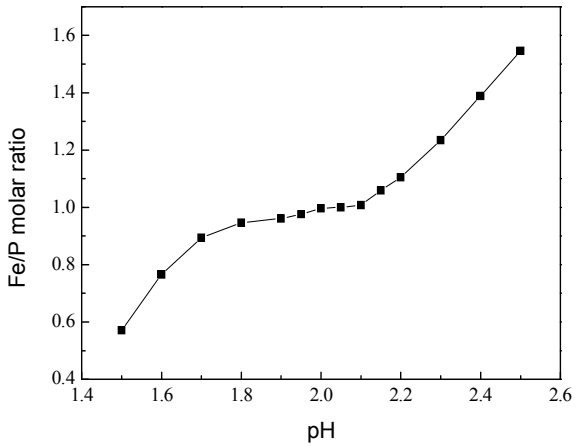

Fig. 5 Effect of pH value on the Fe/P molar ratio of recovered "$FePO_4$"

Table 2 shows the products analyzed detailed ICP-AES analysis of precipitate obtained under pH value of 2. The result shows that the Fe/P molar ratio of precipitate is 1.01, and the overall mass fractions of metal impurities in the products is less than 0.005 %, sulfur content is less than 0.018 %, which is in the range standard values, indicating that high quality of the recovered "$FePO_4$".

Table 2 Quality analysis of the recovered $FePO_4$ in control experiment

	Fe(wt%)	Mg(wt%)	Na(wt%)	K(wt%)	Cu(wt%)	Al(wt%)	Pb(wt%)	S(wt%)	P(wt%)	P/Fe
Standard values[20]	28～30	≤0.005	≤0.005	≤0.005	≤0.001	≤0.005	≤0.0015	≤0.05	15.5～17.0	0.99～1.03
Measured values	29.5	0.003	0.0035	0.0025	0.0006	0.0031	0.0010	0.018	16.6	1.01

Fig. 6 shows the XRD patterns of recovered products from the solution with/without surfactants. Despite of the surfactants added (including the one without adding surfactant), the products show amorphous nature, which is consistent with the literature when the pH value of solution was adjusted to 2.[21] The XRD result has hindered us to determine what the product is. Therefore, to clarify this point, infrared spectroscopy and DSC-TG of the as-precipitated products, and XRD of the annealed products was collected and analyzed.

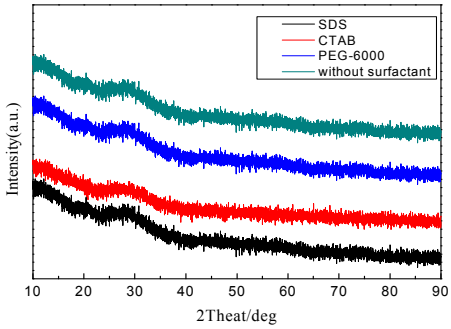

Fig. 6 XRD patterns of recovered $FePO_4$ xH_2O with and without surfactants

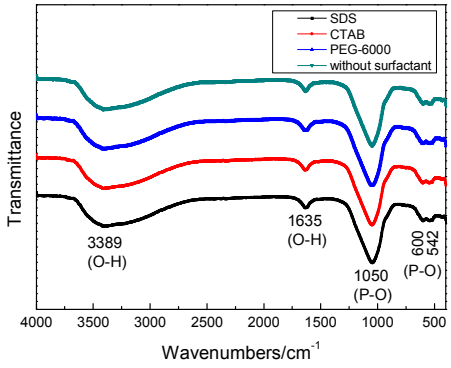

Fig. 7 IR spectra of recovered $FePO_4$ xH_2O with and without surfactants

Infrared spectroscopy is a method to identify molecular structure and compounds according to the relative vibration and rotation of atoms and molecules.[22] Fig. 7 is the infrared spectra of the recycled $FePO_4$. The absorption peaks at 3389 and 1635 cm^{-1} corresponds to the stretching vibration and bending vibration of O-H in the H_2O molecules, which indicated the existence of crystallized water in the recovered sample. While, the absorption peaks at 1050 and 600 cm^{-1} corresponds to telescopic vibration and symmetric bending vibration of P-O in PO_4^{3-}, respectively. The result indicates the recovered sample may be $FePO_4 \cdot xH_2O$.

Fig. 8 is the DSC-TG curve of $FePO_4 \cdot xH_2O$. From the DSC curve we can see that there is an obvious endothermic peak at about 152.45 ^{o}C. TG curve showed there are obvious changes at this range of temperature between the slope curves of 90-200 ^{o}C, indicating that the loss of crystal water changes the mass percentage. From room temperature to 300 °C, TG curve measured a weight loss of about 19.24 %. Complimented with the Fe content from ICP (*i.e.* 29.9 wt %), the recovered sample can be identified as $FePO_4 \cdot 2H_2O$. There appears to be an

exothermic peak at the 670.36 °C in DSC curve, which may indicate a phase transition among the material (e.g. from amorphous into alpha quartz structure).

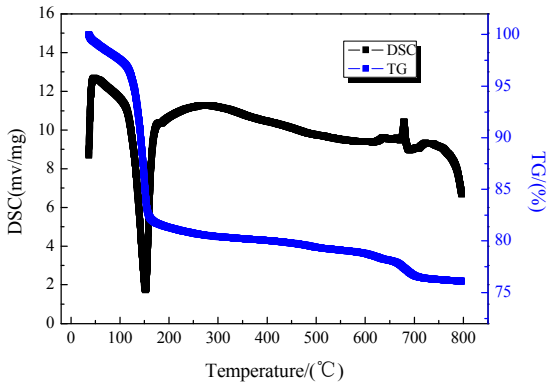

Fig. 8 TG-DSC curves of recycled $FePO_4 \cdot xH_2O$

To further support the analysis from Fig. 8, XRD patterns of recycled amorphous $FePO_4 \cdot 2H_2O$ after being annealed at 700 °C for 5 h was collected and shown in Fig. 9. The diffraction patterns of products match well with $FePO_4$ with alpha quartz structure (PDF#29-0715), the phase transition is consistent with the expectation from DSC-TG analysis. And the unit cell parameters were calculated to be a=0.50330 nm, b=0.50330 nm, c=1.12470 nm, via a least squares fit. Complementary results presented above clearly prove the precipitated products are amorphous $FePO_4 \cdot 2H_2O$.

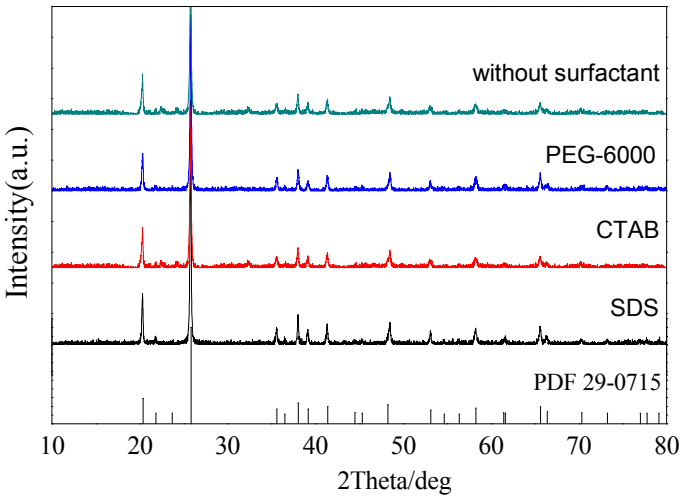

Fig. 9 XRD spectra of $FePO_4$ after heat treatment: A (without surfactant), B (with PEG-6000), C (with CTAB), D

(with SDS)

The SEM images of as-precipitated $FePO_4 \cdot 2H_2O$ are shown in Fig. 10 An severe agglomeration occurred when there is no surfactant added during phase precipitation process. Image C shows CTAB as surfactant for large particle size but agglomeration also exists. Image D shows SDS as surfactant existing in partial reunion. Image B shows the PEG-6000 as surfactant particle size and distribution is more uniform- particle size is smaller and there is no agglomeration. Fig. 10 shows that the size of $FePO_4 \cdot 2H_2O$ particles is reduced when the surface active agent is added.

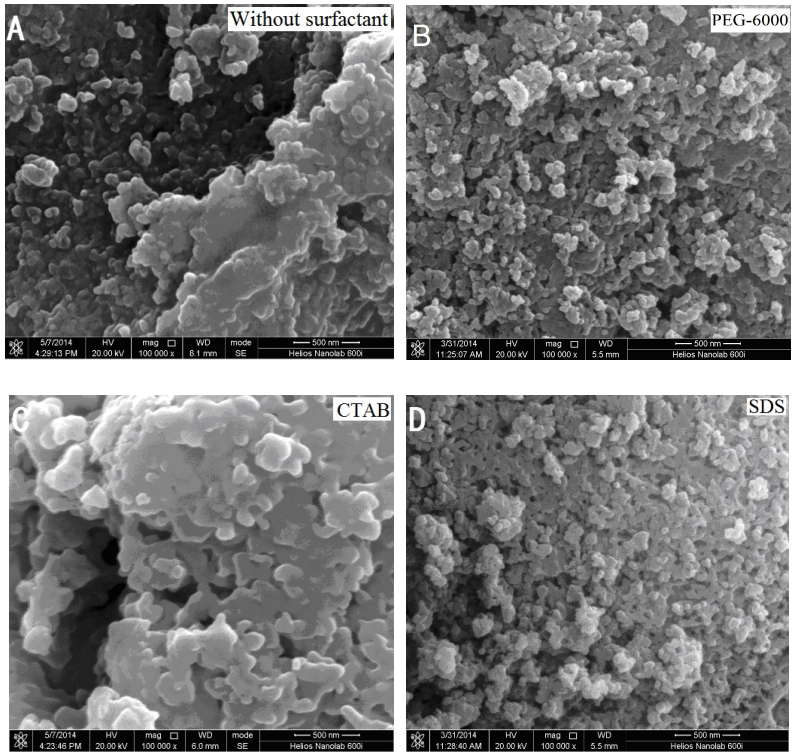

Fig. 10 SEM images of recovery of $FePO_4 \cdot 2H_2O$: A (without surfactant), B (PEG-6000), C (CTAB), and D (SDS)

Fig. 11 shows the magnitudes of Fourier transforms of the k2-weighted EXAFS spectra of Fe K-edge at both TEY and FY mode. While TEY shows information of the surface of the materials (*i.e.* 5-10 nm), FY depicts structural information of bulk material (60 nm under surface).[23] Clearly, when PEG-6000 surfactant was adding during phase precipitation, the recovered $FePO_4 \cdot 2H_2O$ is much more similar to the commercial one comparing to the one

precipitated without adding surfactant. This indicates the higher quality of the recovered $FePO_4$ when PEG-6000 surfactant was added.

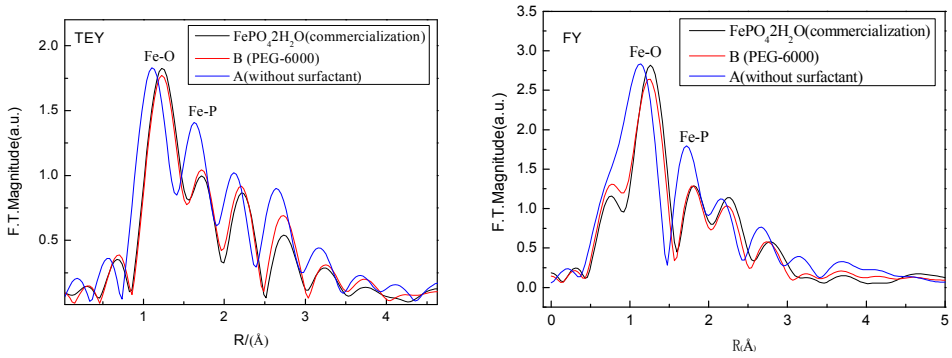

Fig.11 EXAFS analysis of $FePO_4 \cdot 2H_2O$ material

Fig. 12 illustrates the Fe K-edge XANES spectra within $FePO_4 \cdot 2H_2O$. EXAFS curves of the recovered sample show similar characteristics to that of commercial one. When PEG-6000 surfactant is added during phase precipitation, the recovered sample and the commercial $FePO_4 \cdot 2H_2O$ share almost the same spectrum.

The locations on the graph of XANES edge absorption and oxidation state are closely related. This relationship can be used to determine the valence number of the elements because an increase in oxidation state corresponds to a movement of higher energy in absorption. From Fig.12, the absorption graph location of $FePO_4 \cdot 2H_2O$ and B are the same. This means that the iron element has the same valence number.

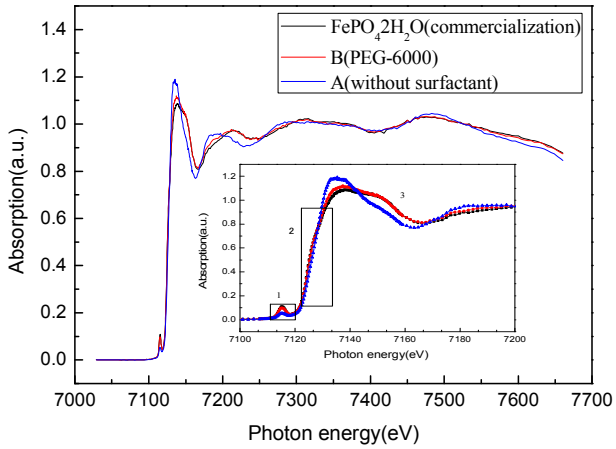

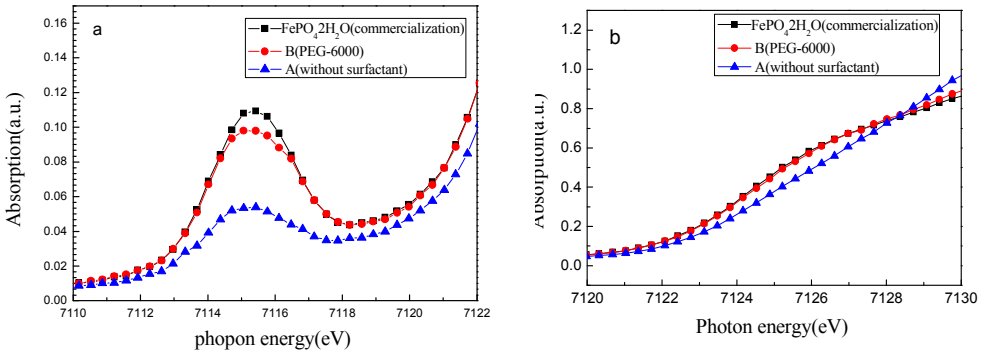

Fig.12 Shows the K-edge XANES spectrum for Fe in $FePO_4 \cdot 2H_2O$ material.

Figure a. is an enlargement of the first rectangle; Figure b. is the enlargement of the second rectangle.

The recovered Li_2CO_3

Fig. 13 clearly shows that the recovered Li_2CO_3 is pure and highly crystalline, as indicated by the well matched patterns to PDF#22-1141 and sharp diffraction peaks, respectively. And the particle size ranges from several microns to about twenty microns.

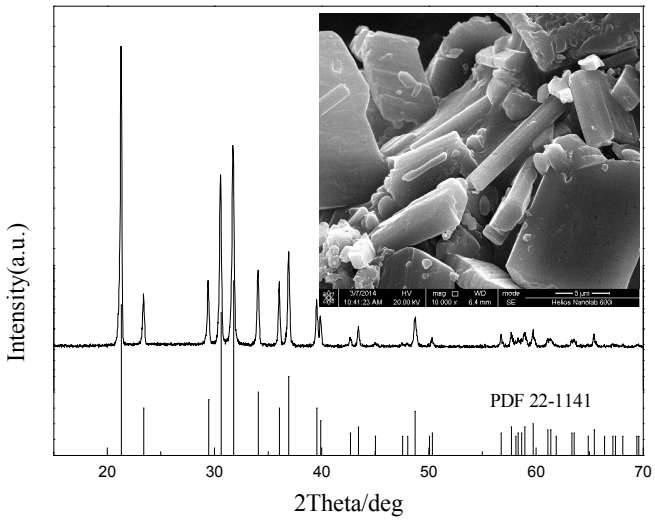

Fig. 13. XRD pattern and SEM images of recovered of Li_2CO_3

Synthesis of $LiFePO_4$/C via carbon thermal reduction using recycled products as raw materials

The recycled $FePO_4 \cdot 2H_2O$ (A, B, C, D) and Li_2CO_3 are used as the raw material to synthesize $LiFePO_4$/C. The obtained $LiFePO_4$/C product were named as A1, B1, C1, D1, which corresponding to using $FePO_4 \cdot 2H_2O$

precipitated under different conditions (i.e. A, B, C, and D). As shown in Fig. 14, as all the synthesized sample can be indexed as $LiFePO_4$ with olivine structure (PDF# 40-1499). We did not find the diffraction peaks of carbon from the XRD diagram, which may be associated with low carbon content and/or its amorphous nature.

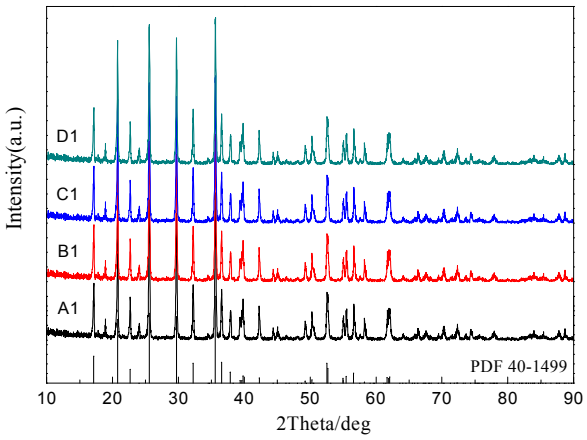

Fig. 14. XRD spectra of the synthesized $LiFePO_4/C$

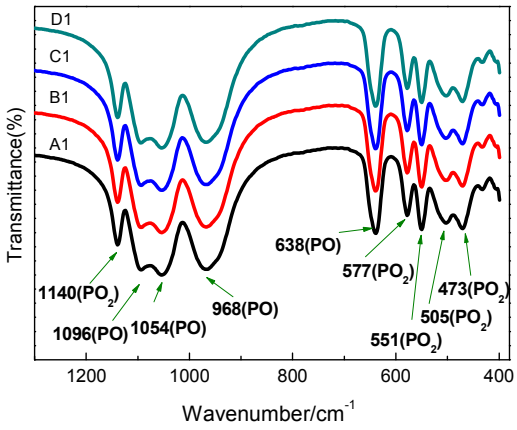

Fig. 15. IR spectra of synthesized $LiFePO_4/C$

Fig. 15 is shows the spectra of all the recycled synthesized sample $LiFePO_4/C$, is constituted by the characteristic peaks of PO_4 group. This spectra is mainly distributed in two spectral bands, namely the strong absorption of 1120-940 cm^{-1} and that of 650-540 cm^{-1}. We can see from Figure Fig. 15 that the group of the PO_2 in 1140cm^{-1} is the stretching vibration and that of 1096 cm^{-1} and 1054 cm^{-1} are the PO anti-symmetric stretching vibration. Wave numbers 968 cm^{-1} and 638 cm^{-1} are symmetric stretching vibration in $LiFePO_4$ PO. 577 cm^{-1} is the anti-symmetric bending vibration in PO_2, and 551 cm^{-1} and 473 cm^{-1} are symmetric bending vibration in PO. Wave

number 505 cm^{-1} is the swing vibration peak in PO_2.[24] In addition, we also can be informed from Fig.15 that the sample is the ideal phase of pure $LiFePO_4$. The existing carbon particles does not affect the spectrum structure of $LiFePO_4$/C.

As can be seem from Fig. 16, the morphology of the synthesized $LiFePO_4$/C can be affected by the different raw materials of $FePO_4 \cdot 2H_2O$ (*i.e.* A, B, C, and D), which is recovered by with/without different surfactants. The synthesized $LiFePO_4$/C using $FePO_4$ B owns smaller smallest particle sizes when compares to synthesized $LiFePO_4$/C using other $FePO_4$ among all the samples, which is believed to beneficial for the electrochemical performance due to the shorter diffusion length of Li^+.

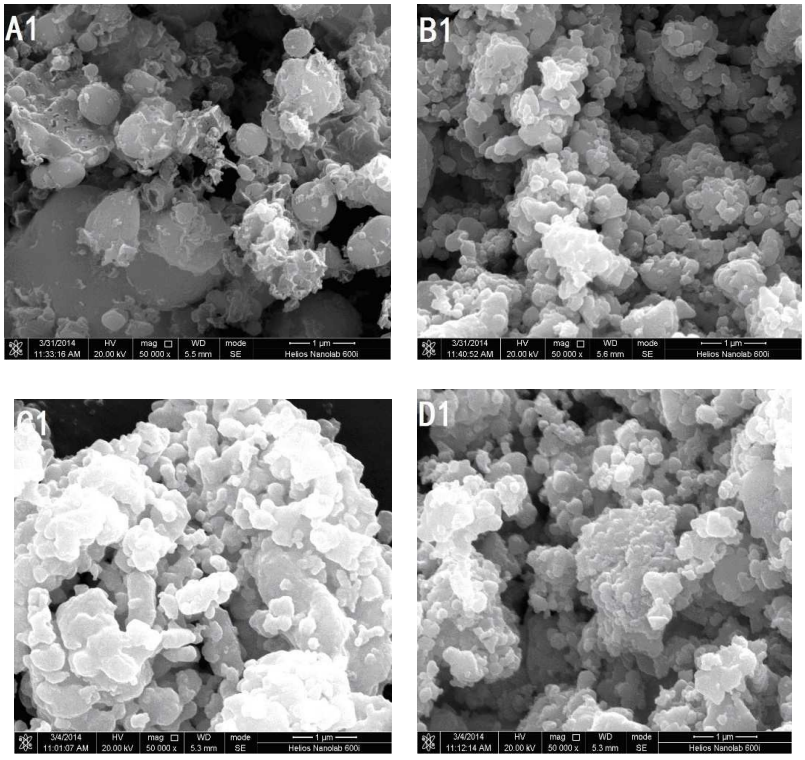

Fig.16. SEM images of synthesized of $FePO_4$/C

Fig. 17 compares the EXAFS graph of resynthesized $LiFePO_4$/C with the addition of surfactant (B1) and commercialized $LiFePO_4$/C. In the perspective of fingerprinting analysis, the oscillation peaks and intensity of B1 and $LiFePO_4$/C are very similar.

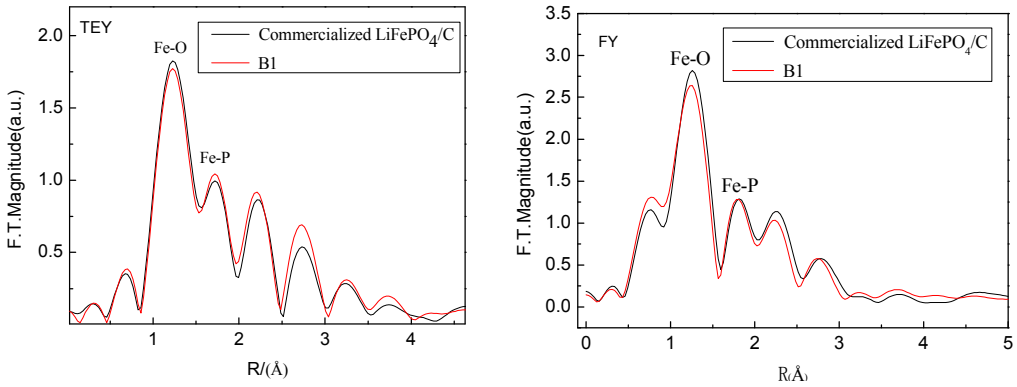

Fig. 17. EXAFS analysis of $LiFePO_4$ material

Fig. 18 shows that the samples have a weak inclination. This means the 3 d orbital of Fe and the 3 p orbital or the p orbital of oxygen form a hybrid.[25] Thus, Fe atoms are from the distorted FeO_6 octahedron. XANES absorption position and oxidation state are closely related. This information can be used to determine the valence number of elements. As oxidation state increases, the absorption energy will also increase. From Fig. 18, the absorption position of $LiFePO_4$/C and other composites are the same. This means Fe element has the same valence number. The XANES can offer qualitative information regarding the three-dimensional structures around the atomic absorption. Because XANES can only detect absorption to 200 eV, there is a better signal-to-noise ratio. Within the appropriate parameters of signal-to-noise ratio, as shown in Figure 18, $LiFePO_4$/C XANES was consistent. This indicates that the Fe within the sample has the same structure, which all have exist in the form of $LiFePO_4$/C.

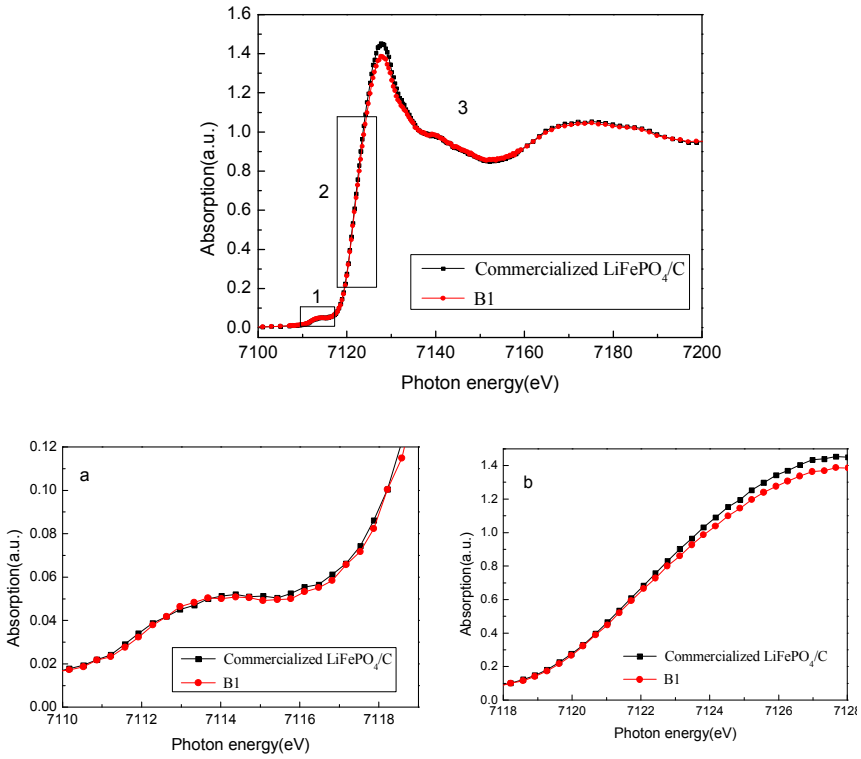

Fig.18. shows the K-edge XANES spectrum for Fe in $LiFePO_4$/C material. （Figure a is an enlargement of the first rectangle from Figure 18. Figure b is the enlargement of the second rectangle from Figure 18.）

The electrochemical performance test of $LiFePO_4$/C

Fig. 19 is the first charge/discharge curve of precursor synthesis of $LiFePO_4$/C (A1, B1, C1, D1) from the recycled $FePO_4$ (A, B, C, D).

The first charge/discharge capacities of B1 are 155.4 $mAh \cdot g^{-1}$ and 153.3 $mAh \cdot g^{-1}$, respectively, which corresponds to initial columbic efficiency of 98.6%. These results are comparable to the performance of $LiFePO_4$ prepared via carbon thermal reduction method using $FePO_4 \cdot 2H_2O$ as iron source in the previous literature.[26] With SDS and CTAB as surfactants, the first discharge capacities are 147.5 $mAh \cdot g^{-1}$ and 133.4 $mAh \cdot g^{-1}$. However, without a surfactant the first discharge capacity was 122.8 $mAh \cdot g^{-1}$. These electrochemical result is consistent with the particle sizes analysis of the samples (shown in Fig. 16), that is smaller particle size leads to better Li^+ diffusion kinetics, thus higher discharge capacity.

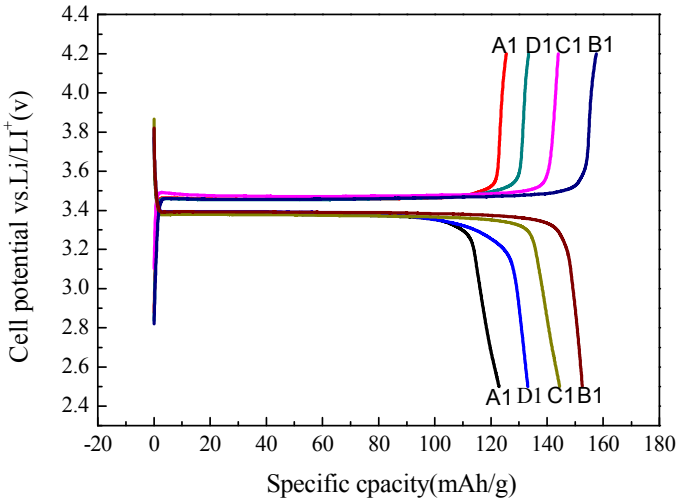

Fig. 19. Charge/discharge curves of $LiFePO_4$/C synthesized using different $FePO_4 \cdot 2H_2O$: A1 (without surfactant), B1 (PEG-6000), C1 (CTAB), and D1 (SDS)

Fig. 20(a) presents the charge/discharge curve of B1 under different current densities. The discharge capacity under 0.2, 0.5, 1, 2, and 5C rates are 152.2 $mAh \cdot g^{-1}$, 150.1 $mAh \cdot g^{-1}$, 137.8 $mAh \cdot g^{-1}$, 120.4 $mAh \cdot g^{-1}$ and 99.8 $mAh \cdot g^{-1}$ respectively. Fig. 20(b) presents the charge/discharge curve of sample commercialized under different current densities. The discharge capacity under 0.2, 0.5, 1, 2, and 5 C rates are 156.8 $mAh \cdot g^{-1}$, 151.3 $mAh \cdot g^{-1}$, 138.2 $mAh \cdot g^{-1}$, 121.5 $mAh \cdot g^{-1}$ and 100.6 $mAh \cdot g^{-1}$ respectively.

The capacity evolution during whole rate test is shown in Fig. 21. It is observed that at 0.1C, 0.2 C, and 0.5 C charge/discharge rates, there is no capacity decays among the 20 cycles; while at 5 C charge/discharge rates, the rate of capacity retention among the 20 cycles was 91.6% and 92.3% respectively. One reason is due to the significant polarization effects. Larger current electrode also distorts the host structure and limits the extraction and insertion of Li^+. Another noteworthy things is that when the current density was reset to 0.1 C, the capacity was almost recovered, indicating a good electrochemical reversibility of the material.

Both the capacity and cyclability of the regenerated sample are comparable to cathode material sample commercialized, while cost is competitive with the market price for the same chemicals prepared from primary resources.

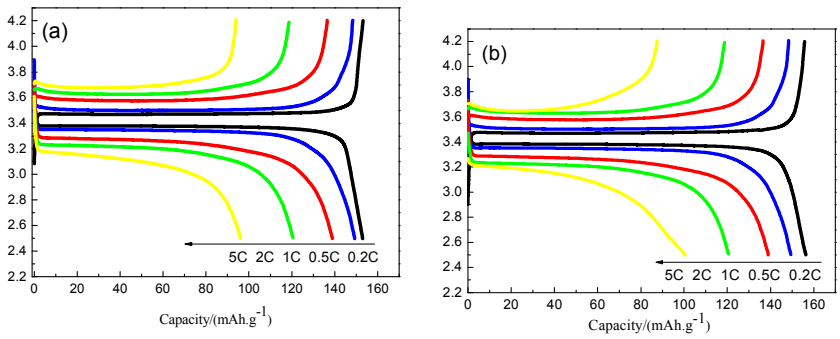

Fig. 20. The charge–discharge curves of the (a) regenerated $LiFePO_4$/C (B1) sample and (b) sample commercialized, between 2.5 and 4.2 V at 0.2, 0.5, 1, 2 and 5 C rate.

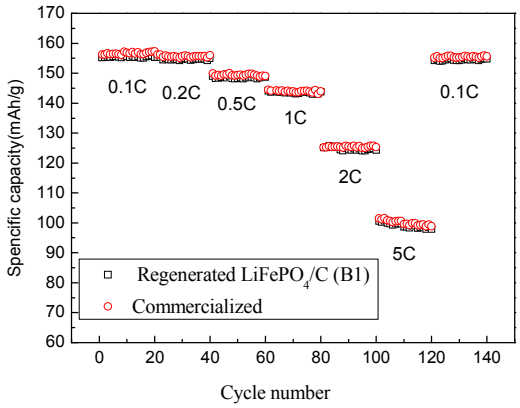

Fig. 21. Rate capability comparison of the regenerated $LiFePO_4$/C (B1) sample and the sample commercialized from pure compound cycled between 2.5 and 4.2 V.

Conclusion

This paper presents a relatively simple recovery process of $FePO_4$ and Li_2CO_3 from waste lithium iron phosphate battery and preparation process of lithium iron phosphate battery cathode materials from recycled material, shown in figure 22. This process includes the following steps: (1) After crushing the discharged battery, recycle the membrane, battery shell and containing copper，(2) A heat treatment anode of 600 °C was conducted to remove coating binder, surface active substances, and carbon. This also oxidizes Fe^{2+} to Fe^{3+}. and aluminum foil is recycled with 0.5mm sieve oscillation sieving, and powders are mixed. (3)The mixed powder was then dissolved in 2.5mol/L sulfuric acid, with the L/S equal to 10, temperature at 60 °C, time of 4h. As a result, 98% of iron and 97% of lithium are leached from the mixed powder. (4) With the PEG-6000 as surfactant, the pH value was

adjusted to 2, causing precipitation of $FePO_4$ (5) The filtrate is concentrated and heated to boiling point. This the results in the precipitation of Na_2CO_3 and Li_2CO_3. (6) The recycled $FePO_4$ is used as the iron source and phosphorus source. Li_2CO_3 is used as lithium source, and sucrose was used as the carbon source. The molar ratio of lithium, iron and phosphorus was set to be 1.05:1:1. Then, the ingredients were milled by the mill ball, dried, and resulting mixture was obtained. (7) The mixture was then pre-sintered in the argon, under the temperature of 350 °C, and calcined under the temperature of 750 °C for 10h to obtain the $LiFePO_4$/C cathode material.

Under the optimized conditions, the recovered $FePO_4$ and Li_2CO_3 crystal has a high purity of products, successfully reaching the standard battery level.

$LiFePO_4$/C was then assembled as a raw material in cathode of half a battery cell. After the battery was subject to an electrochemical performance test, and its resulting electrochemical performance was superb.

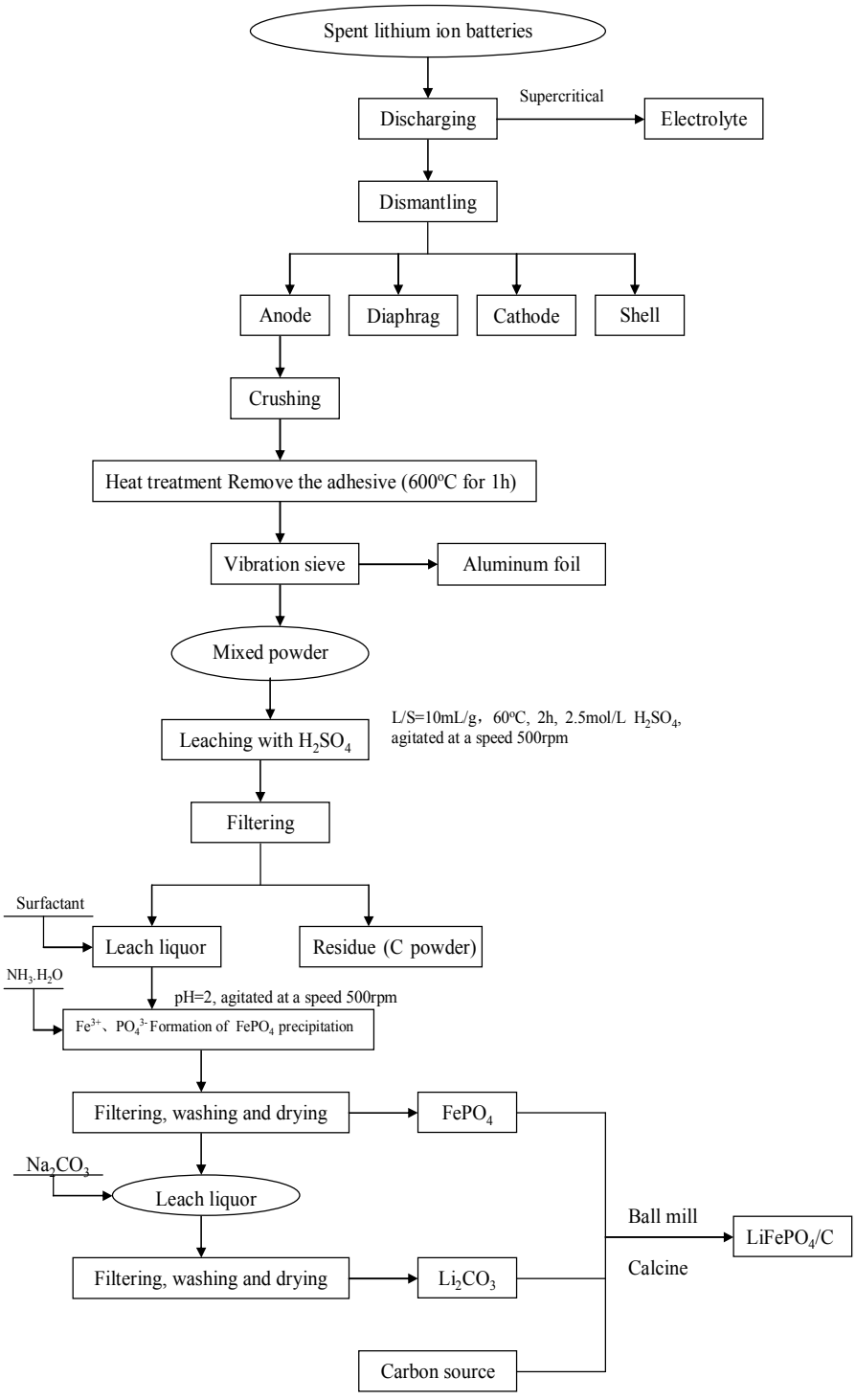

Fig.22. Proposed flow-sheet of spent LIB recycling process

Acknowledgements

This research was supported by the National Natural Science Foundation of China (no. 51274075), the ational Environmental Technology Special Project (no. 201009028), and Guangdong Province-department University-industry Collaboration Project (grant no. 2012B091100315).

Notes and references

1 M. J. Lain, *J. Power Sources*, 2001, 97-98, 736-738.

2 B. Scrosati and J. Garche, *J. Power Sources,* 2010, 195, 2419-2430.

3 D. Ra and K. S. Han, *J Power Sources*, 2006, 163, 1, 284-288.

4 J. Li, P. Shi, Z. Wang, Y. Chena and C. C Chang, *Chemosphere*, 2009, 77,1132-1136.

5 C. K. LEE and K. I. RHEE, *J Power Sources*, 2002, 109, 1, 17–21.

6 L. Chen, X. Tang, Y. Zhang, L. Li, Z. Zeng and Y. Zhang, *Hydrometallurgy*, 2011, 108, 1, 80–86.

7 D. M. Robinson, Y. B. Goreenblatt and G. C. Dismukes, *J Am Chem Soc*, 2010, 132, 33, 11467–11469.

8 D. Song, X. Wang, H. Nie, H. Shi, D. Wang, F. Guo, X. Shi and L. Zhang, *J Power Sources,* 2014, 249, 137-141.

9 T. Zhang, Y. He, F. Wang, L. Ge, X. Zhu and H. Li, *Waste Management,* 2014, 34, 1051-1058.

10 X. Zeng, J. Li and B. Shen, *J Hazard Mater,* 2015, 295, 112-118.

11 E. Gratz, Q. Sa, D. Apelian and Y. Wang, *J Power Sources*, 2014, 262, 255-262.

12 Y. Weng, S. Xu, G. Huang and C. Jiang, *J Hazardous Materials*, 2013, 246-247, 163-172.

13 H. Zou, E. Gratz, D. Apelian and Y. Wang, 2013, 15, 1183 – 1191

14 L. Li, X. Zhang, R. Chen, T. Zhao, J. Lu, F. Wu and K. Amine, *J Power Sources*, 2014, 249, 28-34.

15 X. Liu, H. Li, D. Li, M. Ishida, H. Zhou, *J Power Sources*, 2013, 243, 374-380.

16 http://www.dvdc100.com/v-auto-d-20160112-n-434339829/

17 P. Zhang, T. Yokoyama, O. Itabashi, T. M. Suzuki and I. Katsutoshi, *Hydrometallurgy*, 1998, 47, 259-271.

18 C. Hanisch, T. Loellhoeffel, J. Diekmann, K. J. Markley, W. Haselrieder and A. Kwade, *J Clean Prod,* 2015, 108,

301-311

19 S. Praneetha and A. Vadivel Murugan. RSC Adv, 2013, 3: 25403–25409.

20 A. G. PENG, Z. C. HE and C. Y. YU, *Wu han Inst. Tech*, 2013, 35, 7, 1-5.

21 Y. Huang, H. Ren, Z. Peng and Y. Zhou, *Electrochim. Acta*, 2009, 55, 311-315.

22 R. A. Nyquist and R. O. Kagel, Infrated spectra of inorganic compounds (3800-45 cm^{-1}) [M], New York: Academic Press, 1997.

23 J. R. Croy, M. Balasubramanian ,D. Kim, S. H. Kang and M. M. Thackeray, *Chemistry of materials*. 2011, 23, 5415 –5424.

24 Y. Zhao, L. Peng, B. Liu and G Yu, *Nano Letters*, 2014, 14, 2849–2853.

25 M. S. Chen, S.H. Wu and W. K. Pang. *J Power Sources*, 2013, 241, 690-695.

26 W. Zheng, H. Yu, G. Cao and X. Zhao, *The Chinese Journal of Nonferrous Metals,* 2010, 20, 3, 572–577.